

On Multiscroll Chaotic Attractors in Hysteresis-Based Piecewise-Linear Systems

Fengling Han, Xinghuo Yu, *Senior Member, IEEE*, Yong Feng, and Jiankun Hu

Abstract—This brief analyzes the multiscroll chaotic attractors in hysteresis-based piecewise-linear systems. The dynamics of the chaotic attractors are first analyzed. The unstable limit cycles and the boundary conditions for the occurrence of chaotic behaviors are derived. The sensitivity of systems parameters on the chaotic behaviors is also studied, accompanied by a number of simulations.

Index Terms—Anti-control, chaos, hysteresis, limit cycles, piecewise-linear (PWL) systems.

I. INTRODUCTION

GENERATION of chaos using simple piecewise-linear (PWL) systems has been studied extensively due to their potential applications in, for example, cryptography and biology. A PWL-based random bit generator provides higher security when used in image authentication and public key cryptography [1], [2]. Motivated by fibrillation of the heart, Newcomb *et al.* first studied the chaos generation using a second-order linear system with hysteresis [3]. Saito *et al.* conducted a series of studies in this topic [4]–[8]. Recently, Bizzarri *et al.* gave a bifurcation analysis and experimental validation of the hysteresis-based oscillators [9].

The hysteresis-based chaotic systems have a rather simple structure, making them easier to study with simple tools. The use of the describing function method for analyzing the hysteresis oscillators was explored [10] and the oscillatory dynamics of PWL systems with a single hysteresis was analyzed [11]. A systematic approach for generating multiscroll chaotic attractors using linear systems with switching functions was also proposed [12]–[15] by using which the complexity of behaviors can be increased systematically while maintaining the relative simplicity of the underlying PWL systems. However, the dynamic behaviors in this class of systems have not been fully analyzed.

In this brief, the dynamic behaviors of the multiscroll chaotic systems based on the second-order linear systems with hysteresis series proposed in [13] are thoroughly analyzed. The existence of unstable limit cycles and the boundary conditions for the occurrence of chaos are discussed. The sensitivity of systems dynamics in systems parameters is also studied. Simulation results are presented to validate the results.

Manuscript received September 1, 2006; revised April 17, 2007. This work was supported in part by the Australia Research Council under Grant DP0558791 and Grant LP0455324 and by the National Natural Science Foundation of China under Contract 60474016. This paper was recommended by Associate Editor J. Suykens.

F. Han, X. Yu, and J. Hu are with the Science, Engineering and Technology Portfolio, Royal Melbourne Institute of Technology, Melbourne, Vic. 3001, Australia (e-mail: han.fengling@rmit.edu.au; x.yu@rmit.edu.au; jiankun@rmit.edu.au).

Y. Feng is with the Department of Electrical Engineering, Harbin Institute of Technology, Harbin, 150001, China (e-mail: yfeng@hit.edu.cn).

Digital Object Identifier 10.1109/TCSII.2007.903207

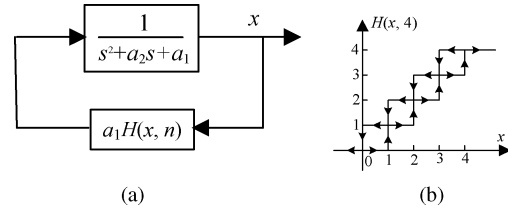


Fig. 1. (a) Second-order linear system with a feedback of hysteresis-series. (b) A hysteresis-series ($n = 4$).

This brief is organized as follows. Section II introduces the hysteresis-series-based PWL systems. The dynamic behaviors of the chaotic attractors are investigated in Section III. Section IV studies the existence of unstable limit cycles which bound the basin of attraction as well as the boundary conditions of the basin of attraction. Section V gives the sensitivity analysis. Conclusions are drawn in Section VI.

II. HYSTERESIS-BASED PWL SYSTEMS

A hysteresis-based PWL system can be constructed using a second-order linear system with a feedback of hysteresis-series as shown in Fig. 1(a), which can be described as follows:

$$\begin{cases} \dot{x} = y \\ \dot{y} = -a_1x - a_2y + a_1u \end{cases} \quad (1)$$

where x and y represent the states, u is the nonlinear state feedback given by

$$u = H(x, n) = \sum_{i=1}^n \text{hys}_i(x) \quad (2)$$

where $H(x, n)$ is the hysteresis-series as shown in Fig. 1(b), n is the number of hystereses.

In order to guarantee the existence of the chaotic motion in system (1), parameters a_1 and a_2 should satisfy

$$\begin{cases} a_2 < 0 \\ a_2^2 - 4a_1 < 0 \end{cases} \quad (3)$$

which gives rise to a pair of complex conjugate eigenvalues with positive real parts that result in useful oscillatory motions for generating chaos. The trajectory of system (1) can be considered as being governed by piecing together trajectory parts in the $(n+1)$ subspaces $S_i = \{(x, y, u) | u = i\}$, $i = 0, \dots, n$ centered at the equilibrium points $(0, 0), (1, 0), \dots, (n, 0)$, respectively.

The solution of system (1) can be solved by defining a state transformation in the i th subspace

$$\begin{cases} x'(t) = x(t) - a_1H(x, i) = x(t) - a_1i \\ y'(t) = y(t) \end{cases}$$

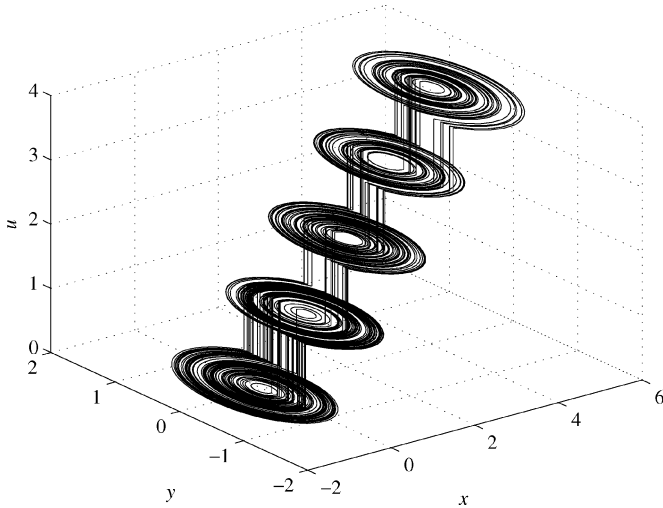


Fig. 2. Trajectory of a five-scroll attractor in x - y - u space ($\alpha_1 = 1$, $\alpha_2 = -0.125$).

which transforms system (1) into the following form:

$$\begin{cases} \dot{x}' = y' \\ \dot{y}' = -a_1 x' - a_2 y'. \end{cases} \quad (4)$$

The solution of system (4) is

$$X'(t) = e^{A(t-t_0)} X'(t_0)$$

where $X' = [x', y']^T$

$$A = \begin{bmatrix} 0 & 1 \\ -a_1 & -a_2 \end{bmatrix} \\ X'(t_0) = \begin{bmatrix} x(t_0) - a_1 i \\ y(t_0) \end{bmatrix}$$

$$e^{At} = e^{\delta t} \begin{bmatrix} \cos(\omega t) - \delta \omega^{-1} \sin(\omega t) & \omega^{-1} \sin(\omega t) \\ -a_1 \omega^{-1} \sin(\omega t) & \cos(\omega t) + \delta \omega^{-1} \sin(\omega t) \end{bmatrix}$$

in which $\delta = -a_2/2$, $\omega = \sqrt{4a_1 - a_2^2}/2$.

Then the formal solution of system (1) can be obtained [see (5) at the bottom of the page]. A five-scroll chaotic attractor from system (1) is shown in Fig. 2 with $a_1 = 1$, $a_2 = -0.125$, $n = 4$.

III. DYNAMIC BEHAVIORS OF THE CHAOTIC ATTRACTORS

Because of the complex conjugate eigenvalues with positive real parts, the linear part of system (1) enables a spirally divergent motion which realizes the “stretching mechanism” while the divergent motion in each subspace can be suppressed with adequately selected hysteresis-series, which can be seen as the “folding mechanism.” In this way, the trajectory of system (1)

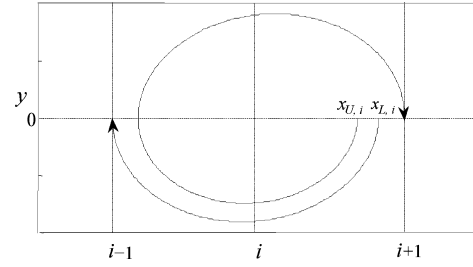


Fig. 3. Critical points around $(i, 0)$ of system (1) ($a_1 = 1$, $a_2 = -0.125$).

can be guaranteed to evolve in different subspaces without converging to any equilibrium point and to remain bounded globally. In this section, the dynamic behaviors of the chaotic attractors generated using system (1) with hysteresis-series (2) are analyzed in detail.

A. Critical Points

There are some critical points that are important for analyzing the dynamic behaviors of the hysteresis-based chaos generator. Because the underlying dynamics is the same except that the equilibrium points lie in different subspaces, without loss of generality, the critical points in the i th subspace are analyzed first, where $i = 0, \dots, n$.

There are two critical points $x_{U,i}$ and $x_{L,i}$ (called the upper and lower critical points, respectively) on the x -axis for the trajectories around each equilibrium point $(i, 0)$ as shown in Fig. 3. A trajectory starting from $(x_{U,i}, 0)$ evolves for 360° to arrive at $(i+1, 0)$. This is considered an extreme point as any trajectory starting from a point on the x -axis greater than $x_{U,i}$ crosses either the upper switching line $x = i+1$ or the lower switching line $x = i-1$, hence activating a new hysteresis function of either $\text{hys}_{i+1}(x)$ or $\text{hys}_{i-1}(x)$, respectively, (by evolving less than 360°). A trajectory starting from $(x_{L,i}, 0)$ evolves 180° to arrive at $(i-1, 0)$. These two critical points determine the following three typical cases of dynamics of system (1).

1) *Case 1:* A trajectory starting from $(x_k, 0)$, where $i < x_k < x_{U,i}$ ($i = 0, \dots, n$) lands on the positive x -axis $(x_{k+1}, 0)$ after evolving 360° around $(i, 0)$. x_{k+1} can be obtained from (5) with initial condition $(x_k, 0)$, $\omega t = 2\pi$

$$x_{k+1} = a_1 i + (x_k - a_1 i) e^{\delta(2\pi/\omega)}, \quad i = 1, \dots, n. \quad (6)$$

2) *Case 2:* A trajectory starting from $(x_k, 0)$, where $x_{U,i} < x_k < x_{L,i}$ ($i = 0, \dots, n$) travels within the i th subspace until it hits its upper switching line $x = i+1$ (evolving between 270° and 360°), then the function $\text{hys}_{i+1}(x)$ is activated.

3) *Case 3:* A trajectory starting from $(x_k, 0)$, where $x_{L,i} < x_k < i+1$ ($i = 0, \dots, n$) travels within the i th subspace until

$$\begin{cases} x(t) = e^{\delta(t-t_0)} (\cos(\omega(t-t_0)) - \delta \omega^{-1} \sin(\omega(t-t_0))) (x(t_0) - a_1 i) \\ \quad + \omega^{-1} e^{\delta(t-t_0)} \sin(\omega(t-t_0)) y(t_0) + a_1 i \\ y(t) = -a_1 \omega^{-1} e^{\delta(t-t_0)} \sin(\omega(t-t_0)) (x(t_0) - a_1 i) \\ \quad + e^{\delta(t-t_0)} (\cos(\omega(t-t_0)) + \delta \omega^{-1} \sin(\omega(t-t_0))) y(t_0) \end{cases} \quad i = 0, \dots, n. \quad (5)$$

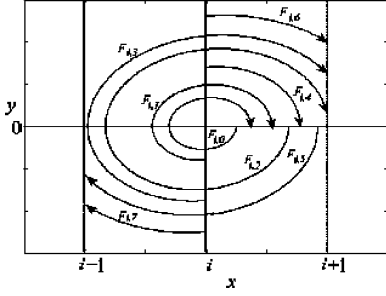


Fig. 4. Eight typical movements of system (1) in the i th subspace.

it hits its lower switching line $x = i - 1$ (evolving between 90° and 180°), then $\text{hys}_{i-1}(x)$ is activated.

The upper and lower critical points around each equilibrium point $(i, 0)$ can be calculated as

$$x_{U,i} = a_1 i + e^{-\delta(2\pi/\omega)} (i + 1 - a_1 i), \quad i = 1, \dots, n \quad (7)$$

$$x_{L,i} = a_1 i - e^{-\delta(\pi/\omega)} (i - 1 - a_1 i), \quad i = 0, \dots, n - 1. \quad (8)$$

For example, for $a_1 = 1$, $a_2 = -0.125$, and $i = 1$, $x_{U,i}$, and $x_{L,i}$ can be obtained from (5) as

$$\begin{aligned} x_{U,1} &= 1 + e^{-\delta(2\pi/\omega)} = 1.675 \\ x_{L,1} &= 1 + e^{-\delta(\pi/\omega)} = 1.821. \end{aligned}$$

The minimum and maximum values of x , i.e., x_{\min} and x_{\max} , of the $(n + 1)$ -scroll on x -axis can be obtained from (5)

$$x_{\min} = -e^{\delta(\pi/\omega)} \quad (9)$$

$$x_{\max} = a_1 n - (n - 1 - a_1 n)e^{\delta(\pi/\omega)}. \quad (10)$$

For example, for $a_1 = 1$, $a_2 = -0.125$, one has

$$x_{\min} = -1.217, \quad x_{\max} = n - x_{\min} = n + 1.217.$$

B. Poincaré Map of the $(n + 1)$ -Scroll Attractors

We now use the Poincaré map to study system (1).

$S_P = \{(x, y) \mid y = 0 \cap (x - i) \geq 0, x \in S_i, i = 0, \dots, n\}$ is chosen as the Poincaré section, and the Poincaré map for system (1) can be expressed by

$$x_{j+1} = M(x_j), \quad j = 0, 1, 2, \dots \quad (11)$$

where x_j and x_{j+1} are coordinates of two consecutive points of the system trajectory on S_P .

Because of the n hysteresis functions in the hysteresis-series, the dynamics of system (1) can be seen as combination of sub-dynamics of system (1) in $(n + 1)$ subspaces. There are basically eight typical types of maps in each subspace $S_i (i = 0, \dots, n)$ as shown in Fig. 4, which are defined as

$$(x_{j+1}, y_{j+1}) = F_{i,k}(x_j, y_j), \quad k = 0, \dots, 7; j = 0, 1, 2, \dots$$

where $F_{i,k}(x_j, y_j)$ represents the map from (x_j, y_j) to (x_{j+1}, y_{j+1}) in the i th subspace with k th type of map.

Note that because of the properties of the hysteresis functions, the trajectory in each subspace S_i always starts on the switching line (being switched from neighboring subplanes S_{i-1} or S_{i+1}) $x = i$, and it will be switched by either lower switching line $x = i - 1$ or upper switching line $x = i + 1$ depending on their positions in relation to the two critical points $x_{U,i}$ and $x_{L,i}$ when landing on x -axis. Each of the eight maps is continuous and can be obtained using (5).

There are three typical scenarios of the Poincaré map M in the $(n + 1)$ subspaces $S_i (i = 0, \dots, n)$: the far left subspace S_0 , the middle subspaces (S_1, \dots, S_{n-1}) and the far right subspace S_n .

In the far left subspace S_0 (i.e., $i = 0$ corresponds to the scroll at the bottom in Fig. 2), for trajectories starting at $(0, y_j)$ being switched from S_1 , there is no lower switching line. Hence, the system state evolves according to Cases 1 and 2 (discussed in Section III-A) around equilibrium $(0, 0)$. The following hitting points can be calculated by the two maps:

$$\begin{cases} (x_{j+1}, 0) = F_{0,1}(0, y_j), & x_{j+1} \leq 1 \\ (1, y_{j+1}) = F_{0,3}(0, y_j), & x_{j+1} > 1 \end{cases} \quad (12-1)$$

where $F_{0,1}(0, y_j)$ stands for the subspace ($i = 0$) with the map for $k = 0$, starting from $(0, y_j)$ to land on $(x_{j+1}, 0)$. $F_{0,3}(0, y_j)$ indicates trajectory starting from $(0, y_j)$ to land at $(1, y_{j+1})$. Then, for starting points on the x -axis, the following hitting points can be calculated using the following two maps:

$$\begin{cases} (x_{j+1}, 0) = F_{0,0}(x_j, 0), & 0 < x_j \leq x_{U,0} \\ (1, y_{j+1}) = F_{0,2}(x_j, 0), & x_{U,0} < x_j \leq 1 \end{cases} \quad (12-2)$$

where $F_{0,0}(x_j, 0)$ stands for the trajectory starting from $(x_j, 0)$ to land at $(x_{j+1}, 0)$ in the subspace ($i = 0$) with the map for $k = 0$ (Case 1); $F_{0,2}(x_j, 0)$ represents Case 2 for a trajectory starting from $(x_j, 0)$ to land at $(1, y_{j+1})$. The second equations in (12-1) and (12-2) describe trajectories switched by upper switching line $x = 1$.

In the middle subspaces $S_i (i = 1, \dots, n - 1)$, a trajectory starting in the i th subspace travels between the neighboring subspaces (either S_{i-1} or S_{i+1}), being switched by either lower switching line $x = i - 1$ or upper switching line $x = i + 1$. Cases 1~3 apply to this scenario. For trajectories switched from S_{i-1} , the following hitting points in S_i can be calculated

$$\begin{cases} (x_{j+1}, 0) = F_{i,4}(i, y_j), & x_{j+1} \leq i + 1 \\ (i + 1, y_{j+1}) = F_{i,6}(i, y_j), & x_{j+1} > i + 1. \end{cases} \quad (13-1)$$

For those trajectories switched from S_{i+1} , the following hitting points are calculated:

$$\begin{cases} (x_{j+1}, 0) = F_{i,1}(i, y_j), & x_{j+1} \leq i + 1 \\ (i + 1, y_{j+1}) = F_{i,3}(i, y_j), & x_{j+1} > i + 1 \\ (i - 1, y_{j+1}) = F_{i,7}(i, y_j), & x_{j+1} \leq i - 1. \end{cases} \quad (13-2)$$

For those trajectories landing on the x -axis via (13-1) and (13-2), the following hitting points can be obtained:

$$\begin{cases} (x_{j+1}, 0) = F_{i,0}(x_j, 0), & i < x_j \leq x_{U,i} \\ (i + 1, y_{j+1}) = F_{i,2}(x_j, 0), & x_{U,i} < x_j < x_{L,i} \\ (i - 1, y_{j+1}) = F_{i,5}(x_j, 0), & x_{L,i} < x_j < i + 1. \end{cases} \quad (13-3)$$

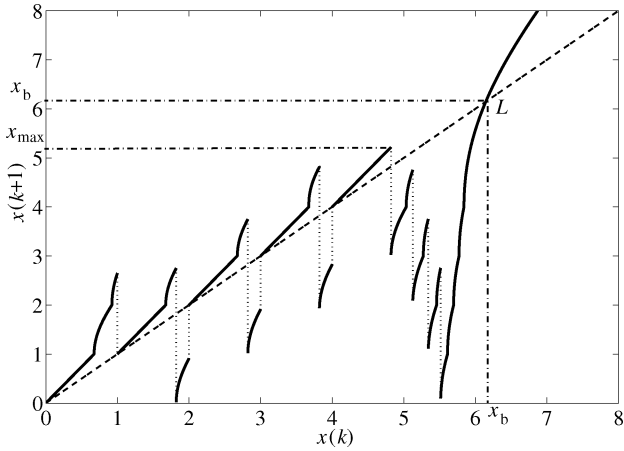


Fig. 5. Poincaré map of a five-scroll chaotic attractor, $n = 4$, $\alpha_1 = 1$, $a_2 = -0.125$.

In the far right subspace S_n , the trajectories are symmetric to those in S_0 . For trajectories starting at switching line $x = n$ from S_{n-1} , there is no upper switching line. Hence, these trajectories evolve according to Cases 1 and 3 around equilibrium $(n, 0)$. The following hitting points can be calculated:

$$(x_{j+1}, 0) = F_{n,4}(n, y_j). \quad (14-1)$$

After hitting the x -axis, the following hitting points are calculated:

$$\begin{cases} (x_{j+1}, 0) = F_{n,0}(x_j, 0), & n < x_j \leq x_{L,n} \\ (n-1, y_{j+1}) = F_{n,5}(x_j, 0), & x_j > x_{L,n}. \end{cases} \quad (14-2)$$

By combining the subdynamics of all subspaces together and recording the consecutive points on Poincaré section, the Poincaré map M can be constructed. The Poincaré map M of a five-scroll attractor is shown in Fig. 5 (due to the tedious expression of each map, their details are omitted here).

In Fig. 5, x_{\max} is the maximum value on the x -axis for the region covered by the scrolls. The trajectory of the five-scroll chaos is bounded even though its equilibrium points are unstable.

IV. BOUNDARY CONDITIONS OF BASIN OF ATTRACTION

There exists an unstable limit cycle (LC) which bounds the basin of attraction of system (1). This section is devoted to the study of the boundary conditions of the basin of attraction.

In Fig. 5, point L corresponds to a trajectory of LC. If $x_{\max} < x_b$ (x_b is the positive x -coordinate of LC when $y = 0$), the trajectory of system (1) will remain bounded. The trajectory of LC can be determined by linking together subtrajectories in the $n+1$ subspaces separated by the $n+1$ switching lines $x = 0, 1, \dots, n$ (corresponding to the $n+1$ hysteresis outputs). This cycle can be derived by starting at $X^*(x, y)$ in a subspace and then letting the trajectory travel across all subspaces successively until it hits the same point $X^*(x, y)$ again. There are a number of ways of calculating the LC. One simple way is to start at a point $(0, y_a)$ on the negative y -axis as shown in Fig. 6. According to the symmetry, and to use the typical maps successively to find the LC when it returns to the same point $(0, y_a)$

$$F_{n-1,6}(F_{n-2,6}(\dots F_{2,6}(F_{1,6}(F_{0,3}(0, y_a)))))) = (n, -y_a). \quad (15)$$

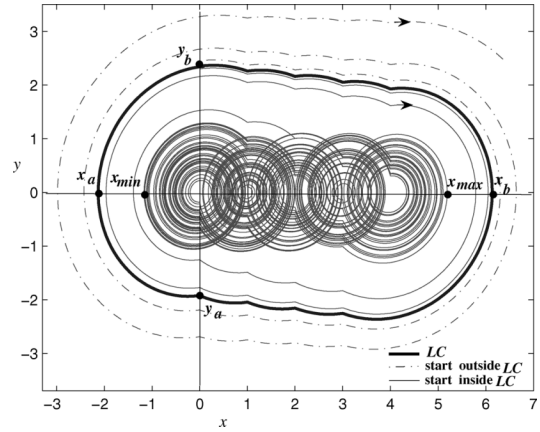


Fig. 6. Trajectory starts close to the boundary of basin of attraction.

TABLE I
COORDINATES ON x - AND y -AXES OF LIMIT CYCLE ($a_1 = 1$, $a_2 = -0.125$)

| n | 1 | 2 | 4 | 5 | 8 | 10 | 12 |
|-------|--------|--------|--------|--------|--------|--------|--------|
| y_a | -1.169 | -1.528 | -1.933 | -2.071 | -2.353 | -2.484 | -2.584 |
| x_a | -1.295 | -1.693 | -2.139 | -2.295 | -2.606 | -2.752 | -2.861 |
| y_b | 1.422 | 1.860 | 2.353 | 2.521 | 2.863 | 3.023 | 3.145 |
| x_b | 2.295 | 3.693 | 6.139 | 7.295 | 10.606 | 12.752 | 14.861 |

From the Poincaré map shown in Fig. 5, it can also be observed that the LC is unique and unstable. Any trajectory starting from either side of the LC will not converge to it. A trajectory starting inside LC will stay within the area enclosed by the LC. In this sense, the LC constitutes the boundary of the basin of attraction. Some typical trajectories of the five-scroll attractor are also shown in Fig. 6. Starting from initial condition $(0, 2.30)$ ($y_b = 2.35$), the trajectory will settle in scroll chaos (see the region covered with scrolls in Fig. 6) after the following mapping sequence: $F_{0,6}, F_{1,6}, F_{2,6}, F_{3,6}, F_{4,4} + F_{4,5}, F_{3,7}, F_{2,7}, F_{1,7}, F_{0,3}, F_{1,6}, F_{2,6}, F_{3,6}, F_{4,4} + F_{4,5}, F_{3,7}, F_{2,7}, F_{1,7}, F_{0,3}, F_{1,6}$. For another initial condition $(0, 2.45)$ which is outside the LC, the trajectory will diverge to infinity.

The contour of LC can be determined if any particular point on the LC is known. This can be done via a lookup table based on y_a . Supposing that the LC starts on $(0, y_a)$, x_a can be obtained from (5)

$$\begin{cases} x_a = y_a \omega^{-1} e^{\delta t} \sin(\omega t) \\ \tan(\omega t) = -\omega \delta^{-1} \end{cases} \quad (16-1)$$

and based on x_a and y_a , x_b and y_b can be obtained with

$$\begin{cases} y_b = -y_a e^{\delta \pi \omega^{-1}} \\ x_b = n - x_a. \end{cases} \quad (16-2)$$

With the specific parameters $a_1 = 1$, $a_2 = -0.125$, when $n = 1, 2, 4, 5, 8, 10$, and 12 , respectively, the x_a , y_a , x_b , and y_b of $(n+1)$ -scroll attractors are shown in Table I. From Table I, one can see an overall picture of LC with different n .

V. SENSITIVITY ANALYSIS

In this section, the sensitivity of the system parameters on the dynamic behaviors is investigated.

The dynamics of system (1) depends on the parameters a_1 , a_2 , and n . The stability of system (1) can also be determined by the relationship between x_{\max} and x_b as shown in Fig. 6.

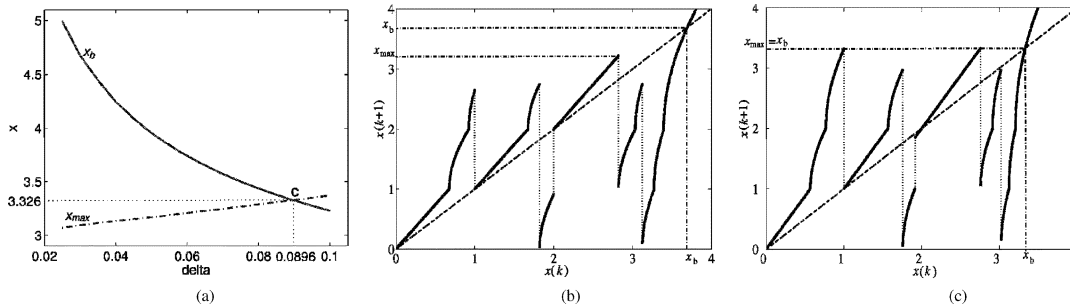


Fig. 7. (a) x_{\max} and x_b versus δ ($n = 2$). (b) Poincaré map of system (1), $n = 2$, $\alpha_1 = 1$, $a_2 = -0.125$. (c) Poincaré map of system (1), $n = 2$, $\alpha_1 = 1$, $a_2 = -0.1792$.

A. n and a_1 Fixed, a_2 Varies

When n and a_1 are fixed, both x_b and x_{\max} vary with respect to a_2 or δ ($\delta = -a_2/2$). Based on (10) and (16), x_b decreases and x_{\max} increases with the increase of δ . x_{\max} and x_b versus δ when $n = 2$, $a_1 = 1$ are shown in Fig. 7(a) which clearly demonstrates this phenomena. Therefore, the system dynamics may change from bounded (chaotic) to unstable motion because the size of the basin of attraction becomes smaller (x_b decreases) and x_{\max} becomes larger with the increase of δ . The Poincaré map of system (1) when $n = 2$, $a_1 = 1$, $a_2 = -0.125$ is shown in Fig. 7(b) which indicates $x_{\max} < x_b$, the trajectory stays within the basin of attraction if the initial values are within it. When δ is increased to 0.0896 ($a_2 = -0.179$), the critical case $x_{\max} = x_b$ appears. Its Poincaré map is shown in Fig. 7(c). Point C in Fig. 7(a) corresponds to the critical point.

The conditions for the critical case can be obtained with (10) and (16) as

$$\begin{cases} e^{\delta\pi/\omega} = -y_a\omega^{-1} \cdot e^{\delta t} \sin(\omega t) \\ \tan(\omega t) = -\omega\delta^{-1}. \end{cases} \quad (17)$$

When $a_1 = 1$, $n = 2$, one can obtain, for $\delta = 0.0896$ ($a_2 = -0.179$), $x_{\max} = x_b = 3.326$. If a_2 is further decreased, the trajectory will escape from the basin of attraction, the unstable dynamics appears.

B. a_1 and a_2 Fixed, n Varies

When $a_1 = 1$ and a_2 is fixed x_{\max} $x_b = n + y_a(n) = n + \Delta(n)$ with the increase of n , the system will change from an unstable motion to a bounded motion because the increase of x_b is larger than that of x_{\max} . For example, when $n = 2$, $a_1 = 1$, $a_2 = -0.2$, the trajectory of system (1) is unstable. If n is increased to 4, a_1 and a_2 are kept unchanged, the size of the basin of attraction will increase faster than that of x_{\max} , and chaos will appear.

VI. CONCLUSION AND FUTURE WORK

In this brief, the dynamic behaviors of multiscroll chaotic attractors in the hysteresis-based second-order linear systems have been thoroughly studied with a number of simulations presented to validate the analysis.

Chaotic cryptosystems have the potential in improving biometric image related security [16], [17]. Our future work will

focus on improving unpredictability of the encrypted image [18] using the idea of true random bit generator [1].

REFERENCES

- [1] M. E. Yalcin, J. A. K. Suykens, and J. Vandewalle, "True random bit generation from a double scroll attractor," *IEEE Trans. Circuits Syst. II, Exp. Briefs*, vol. 51, no. 7, pp. 1395–1404, Jul. 2004.
- [2] T. Addabbo, M. Alioto, A. Fort, S. Rocchi, and V. Vignoli, "Low-hardware complexity PRBGs based on a piecewise-linear chaotic map," *IEEE Trans. Circuits Syst. II, Exp. Briefs*, vol. 53, no. 5, pp. 329–333, May 2006.
- [3] R. W. Newcomb and S. Sathyan, "An RC op amp chaos generator," *IEEE Trans. Circuits Syst. I, Fundam. Theory Appl.*, vol. 30, no. 1, pp. 54–56, Jan. 1983.
- [4] T. Saito, "On a hysteresis chaos generator," in *Proc. IEEE ISCAS*, 1985, pp. 847–849.
- [5] T. Suzuki and T. Saito, "On fundamental bifurcations from a hysteresis hyperchaos generator," *IEEE Trans. Circuits Syst. I, Fundam. Theory Appl.*, vol. 41, no. 12, pp. 876–884, Dec. 1994.
- [6] T. Saito and S. Nakagawa, "Chaos from a hysteresis and switched circuit," *Phil. Trans. R. Soc. Lond. A*, vol. 353, no. 1701, pp. 47–57, 1995.
- [7] T. Saito and K. Mitsubori, "Control of chaos from a piecewise linear hysteresis circuit," *IEEE Trans. Circuits Syst. I, Fundam. Theory Appl.*, vol. 42, no. 3, pp. 168–172, Mar. 1995.
- [8] M. Kataoka and T. Saito, "A 2-port VCCS chaotic oscillator and quad screw attractor," *IEEE Trans. Circuits Syst. I, Fundam. Theory Appl.*, vol. 48, no. 2, pp. 221–225, Feb. 2001.
- [9] F. Bizzarri, D. Stello, and M. Storage, "Bifurcation analysis and its experimental validation for a hysteresis circuit oscillator," *IEEE Trans. Circuits Syst. I, Reg. Papers*, vol. 53, no. 5, pp. 517–521, May 2006.
- [10] M. Bonnin, M. Gilli, and P. P. Civalleri, "A mixed time-frequency-domain approach for the analysis of a hysteretic oscillator," *IEEE Trans. Circuits Syst. II, Exp. Briefs*, vol. 52, no. 9, pp. 525–529, Sep. 2005.
- [11] U. F. Moreno, P. L. D. Peres, and I. S. Bonatti, "Analysis of piecewise-linear oscillators with hysteresis," *IEEE Trans. Circuits Syst. I, Fundam. Theory Appl.*, vol. 50, no. 8, pp. 1120–1124, Aug. 2003.
- [12] J. Lü and G. Chen, "Generating multi-dimensional scroll chaotic attractors: Theories, methods and applications," *Int. J. Bifurca. Chaos*, vol. 16, no. 6, pp. 775–858, 2006.
- [13] F. Han, X. Yu, X. Wang, Y. Feng, and G. Chen, "N-scroll chaotic oscillators by second-order systems and double-hysteresis blocks," *Electron. Lett.*, vol. 39, no. 23, pp. 1636–1637, 2003.
- [14] J. Lü, F. Han, X. Yu, and G. Chen, "Generating multi-dimensional scroll chaotic attractors: A hysteresis series switching method," *Automatica*, vol. 40, no. 10, pp. 1677–1687, 2004.
- [15] M. E. Yalcin, J. A. K. Suykens, and J. Vandewalle, "Families of scroll grid attractors," *Int. J. Bifurca. Chaos*, vol. 12, no. 1, pp. 23–41, 2002.
- [16] X. Yi, "Hash function based on chaotic tent maps," *IEEE Trans. Circuits Syst. II, Exp. Briefs*, vol. 52, no. 6, pp. 354–357, Jun. 2005.
- [17] D. Xiao, X. Liao, and K. Wong, "Improving the security of a dynamic look-up table based chaotic cryptosystem," *IEEE Trans. Circuits Syst. II, Exp. Briefs*, vol. 53, no. 6, pp. 502–506, Jun. 2006.
- [18] F. Han, J. Hu, X. Yu, and Y. Wang, "A new fingerprint image encryption approach based on two-dimensional chaotic attractors," *Int. J. Appl. Math. Comput.*, vol. 185, pp. 931–939, 2007.